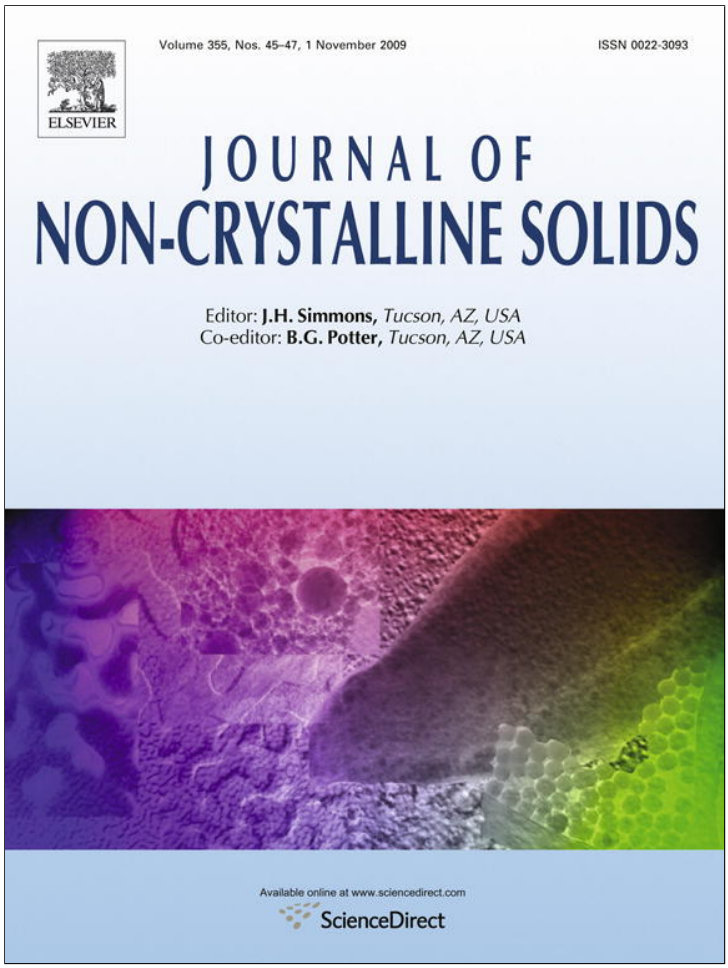

Journal of Non-Crystalline Solids 355 (2009) 2295–2301

Contents lists available at ScienceDirect

Journal of Non-Crystalline Solids

journal homepage: www.elsevier.com/locate/jnoncrysol

Controlled crystallization and ionic conductivity of a nanostructured $LiAlGePO_4$ glass–ceramic

Ana Milena Cruz [1], Eduardo Bellini Ferreira [2], Ana Candida M. Rodrigues *

Universidade Federal de São Carlos, Departamento de Engenharia de Materiais, Rod. Washington Luis Km 235, São Carlos 13565-905, SP, Brazil

ARTICLE INFO

Article history:
Received 10 February 2009
Received in revised form 11 July 2009
Available online 19 August 2009

PACS:
64.70.kj
64.70.kp
66.10.Ed

Keywords:
Glass–ceramics
Conductivity
Fast ion conduction

ABSTRACT

A $Li_{1.5}[Al_{0.5}Ge_{1.5}(PO_4)_3]$ glass composition was subjected to several crystallization treatments to obtain glass–ceramics with controlled microstructures. The glass transition (T_g), crystallization onset (T_x) and melting (T_m) temperatures of the parent glass were characterized by differential scanning calorimetry (DSC). The glass has a reduced glass transition temperature $T_{gr} = T_g/T_m = 0.57$ indicating the possibility of internal nucleation. This assumption was corroborated by the similar DSC crystallization peaks from monolithic and powder samples. The temperature of the maximum nucleation rate was estimated by DSC. Different microstructures were produced by double heat treatments, in which crystal nucleation was processed at the estimated temperature of maximum nucleation rate for different lengths of time. Crystals were subsequently grown at an intermediate temperature between T_g and T_x. Single phase glass–ceramics with Nasicon structures and grain sizes ranging from 220 nm to 8 μm were then synthesized and the influence of the microstructure on the electrical conductivity was analysed. The results showed that the larger the average grain size, the higher the electrical conductivity. Controlled glass crystallization allowed for the synthesis of glass–ceramics with fine microstructures and higher electrical conductivity than those of ceramics with the same composition obtained by the classical sintering route and reported in literature.

1. Introduction

Ceramics with Nasicon (Na Super Ionic Conductor) structures have been widely investigated due to their high ionic conductivity and potential use as solid electrolytes. Their lithium homologues, in particular, may be used in electrochemical devices such as batteries [1] and sensors [2]. These ceramics are usually obtained by the classical powder sintering route and several compositions have been synthesized and studied [3–9]. Alternatively, Nasicon ceramics have been obtained successfully by other synthesis routes such as sol–gel [2,10] and glass–ceramic processes [11–17]. The latter, which do not require the sintering step, produce materials with homogeneous microstructures and low porosity. Nevertheless, in the referenced studies, glass–ceramics were obtained by treating glasses at the crystallization peak temperature measured by differential scanning calorimetry (DSC) for periods as long as 12 h [12–16] or 24 h [11] without optimizing the heat treatment parameters and, hence, the resulting microstructures. Double heat treatments, i.e. successive treatments for crystal nucleation and growth at different temperatures, were also employed but with no attempt to control the microstructures [11,17].

This paper presents a previous characterization of the precursor glass to ascertain its nucleation tendency (internal or surface), its temperature of maximum nucleation rate and its thermal stability. Knowledge of the above characteristics is necessary to control the crystallization of the precursor glass and obtain different microstructures. Accordingly, the glass–ceramics were synthesized by double heat treatments with an optimized nucleation step followed by growth at a higher temperature. The glass with the $Li_{1.5}[Al_{0.5}Ge_{1.5}(PO_4)_3]$ composition was chosen due to the possibility of obtaining a Nasicon structure as the single phase [13]. Also, in this composition, the partial substitution of tetravalent germanium by trivalent aluminum allows more Li^+ into the crystal structure and, therefore, increased ionic conductivity [5]. The lithium–ion conductivity of the resulting glass–ceramics was measured by impedance spectroscopy and the influence of the microstructure on the ionic conductivity is discussed.

2. Experimental and methods

2.1. Glass precursor preparation

The $Li_{1.5}[Al_{0.5}Ge_{1.5}(PO_4)_3]$ precursor glass was obtained by melting a mixture of reagent grade Li_2CO_3, GeO_2, Al_2O_3 and $NH_4H_2PO_4$

* Corresponding author. Tel.: +55 16 3351 8524; fax: +55 16 3361 5404
E-mail address: acmr@ufscar.br (A. C. M. Rodrigues).
[1] Now working in the Instituto de Ciencia de Materials de Barcelona Campus de la UAB, E-08193 Bellaterra Barcelona, Espanha.
[2] Now working in the Departamento de Materiais e Tecnologia, Faculdade de Engenharia, UNESP, 12516-410 Guaratinguetá, SP, Brazil.

0022-3093/$ - see front matter © 2009 Elsevier B.V. All rights reserved.
doi:10.1016/j.jnoncrysol.2009.07.012

Table 1
Nominal and experimental glass composition and chemical formulas.

	Weight%				Chemical formula
	Li_2O	Al_2O_3	GeO_2	P_2O_5[a]	
Nominal composition	5.4	6.1	37.5	51.0	$Li_{1.5}[Al_{0.5}Ge_{1.5}(PO_4)_3]$
Experimental composition – batch 1	5.3	5.8	41.4	47.6[a]	$Li_{1.5}[Al_{0.48}Ge_{1.7}(PO_4)_{2.8}]$
Experimental composition – batch 2	5.3	5.6	40.4	48.7[a]	$Li_{1.5}[Al_{0.48}Ge_{1.6}(PO_4)_{2.9}]$

[a] P_2O_5 content was calculated by difference.

in the proportions of the stoichiometric formula. The mix of raw materials was homogenized in a planetary ball mill (with Si_3N_4 balls and jar) for 2 min at 500 rpm. The mixture was then melted at 1200 °C for 30 min in an alumina crucible. Platinum crucibles are not suitable since they can be corroded by phosphorus compounds. The resulting low viscosity liquid was splat-cooled between stainless steel plates and the quenched glass annealed at 470 °C for 2 h to relieve thermal stresses. After cooling, the glass was bubble-free, transparent and colorless. No corrosion of the alumina crucible was visible.

2.2. Glass and glass–ceramics characterization

The chemical composition of the glass was determined by inductively coupled plasma optical emission spectrometry (ICP OES). An extra batch of glass was melted to verify the reproducibility of the synthesis procedure. The slight differences between nominal and experimental values in Table 1 can be considered nonsignificant for our purposes. The equivalence between the two batches indicates that the synthesis procedure adopted is reproducible. Electrical measurements were taken in samples from only one batch, and hereinafter we refer only to the nominal $Li_{1.5}[Al_{0.5}Ge_{1.5}(PO_4)_3]$ composition. The lower than nominal proportion of Al_2O_3 is consistent with the absence of crucible attack by the melt.

Glass and glass–ceramic densities were measured by picnometry in water at room temperature, with an estimated accuracy of 2%. X-ray diffractions were obtained in a Siemens D5000 diffractometer with Cu Kα radiation and a scan speed of 2°/min. SEM micrographs were obtained using a Phillips XL scanning electron microscope equipped with a field emission gun (FEG).

DSC analysis (Netzsch DSC 404) was performed at a heating rate of 10 °C/min, using platinum pans and covers. The following characteristic temperatures of the precursor glasses were taken from the DSC curves: the glass transition temperature (T_g), the crystallization onset (T_x – obtained by the intercept of the extrapolated base line and the peak trace on its low temperature side), and the endpoint of the melting peak (T_m). It should be kept in mind that T_g appears in the DSC curve as a step-like endothermically oriented change in the baseline when, upon heating, the sample changes from a hard, solid-like state to a super-cooled liquid. A heat capacity increase follows the change from solid to liquid and provokes the change in the baseline at the DSC trace.

2.3. Assessment of the temperature of maximum nucleation rate

The temperature of the maximum nucleation rate was estimated by a method proposed by Ray and Day [18], which is currently employed in the literature (e.g. [19]). By this method, samples previously nucleated at different temperatures above and below T_g for a constant period of time are subjected to DSC runs at a fixed rate. The resulting crystallization peaks are observed at different temperatures, depending on the nuclei concentration achieved – the higher the nuclei concentration the lower the crystallization peak temperature. Plotting the inverse of the temperature of the DSC crystallization peak against the temperature of previous nucleation, one observes a maximum at the temperature of maximum nuclei concentration, which corresponds to the temperature of the maximum nucleation rate (T_{max}).

The previous isothermal heat treatments for nucleation lasted 2 h. After the nucleation treatments, the DCS analyses were run at 10 °C/min. A further study of the optimal duration of growth at 571 °C of samples subjected to different nucleation time intervals at 524 °C was conducted by means of isothermal DSC analyses.

2.4. Electrical measurements

Electrical conductivity was measured by impedance spectroscopy (Solartron 2016 impedance analyzer) in a two-electrode configuration cell in air, in the 0.1–10^6 Hz frequency range, with voltage amplitude of 500 mV. Measurements were taken from room temperature to 120 °C. The samples were about 0.1 cm thick and had a contact area of 0.05–0.1 cm^2. After polishing, gold was sputtered onto the two parallel faces of the samples in order to ensure the necessary electrical contacts.

3. Results

3.1. Density and DSC analysis

Table 2 lists the measured densities of the glass and glass–ceramics, while Fig. 1 shows DSC curves of monolithic and powder samples with particle sizes ranging from 100 to 177 μm.

3.2. Assessment of the maximum nucleation rate temperature

The DSC curves of samples subjected to different previous nucleation heat treatments are shown in Fig. 2. In the present case, samples were previously heat treated for 2 h at temperatures (°C) of $T_g - 10$, $T_g - 20$, T_g, $T_g + 10$ and $T_g + 20$ and then subjected to dynamic DSC runs at 10 °C/min. Plotting the inverse of the DSC crystallization peak temperature against the temperature of previous nucleation heat treatment (Fig. 3) reveals an apparent saturation after approximately 524 °C, which coincides with the DSC glass transition temperature and is assumed to be approximately the temperature of maximum nucleation rate (T_{max}). In the Section 4 we analyze this assumption in detail.

Table 2
Density of $Li_{1.5}[Al_{0.5}Ge_{1.5}(PO_4)_3]$ glass and glass–ceramics.

Sample	Density (g/cm^3)
Glass	2.98 ± 0.06
Glass–ceramic obtained at 524 °C for 48 h + 571 °C for 30 min	3.23 ± 0.06
Glass–ceramic obtained at 618 °C for 30 min	3.15 ± 0.06

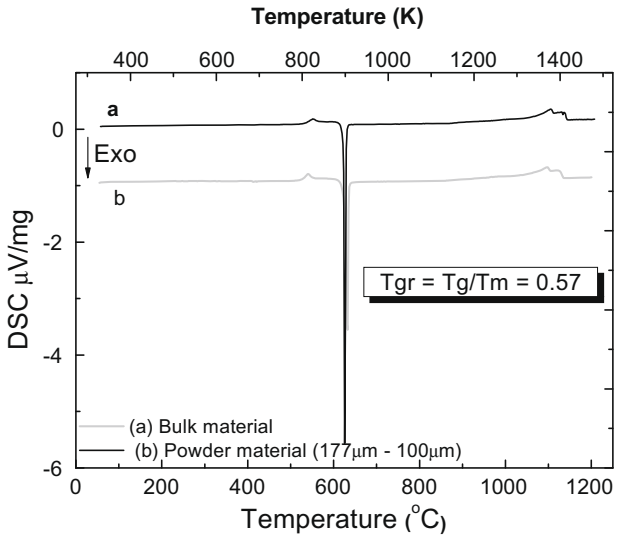

Fig. 1. DSC curves of $Li_{1.5}[Al_{0.5}Ge_{1.5}(PO_4)_3]$ glass, (a) monolithic and (b) powder samples.

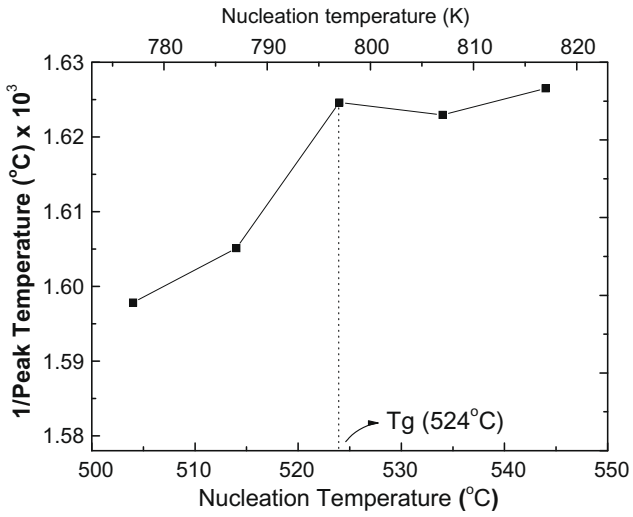

Fig. 3. Inverse of DSC crystallization peak temperatures of previously nucleated samples as a function of the nucleation temperature of the $Li_{1.5}[Al_{0.5}Ge_{1.5}(PO_4)_3]$ glass. Line is drawn as guide to the eyes.

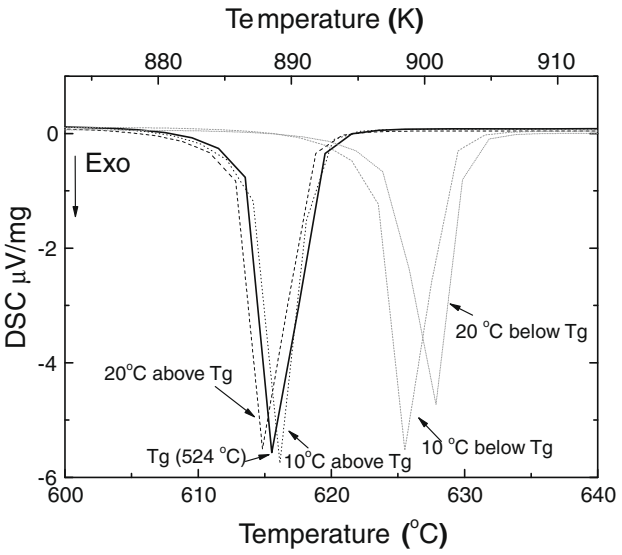

Fig. 2. Dynamic DSC curves of samples previously heat treated for 2 h at the indicated temperatures.

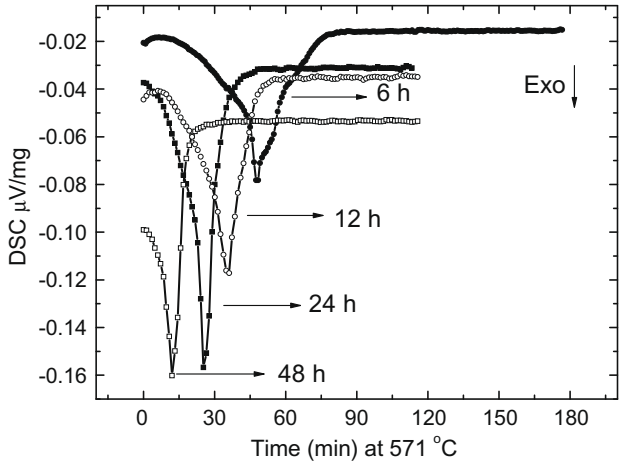

Fig. 4. Isothermal (571 °C) DSC curves of glass samples previously nucleated at T_g (524 °C) for the indicated periods.

3.3. Glass–ceramic synthesis

Double heat treatments, i.e., a nucleation step at 524 °C performed for different time intervals (6, 12, 18, 24 and 48 h), followed by a growth step at 571 °C, were applied to obtain glass–ceramics with different nanoscale grain sizes. The crystal growth temperature was taken as 571 °C, which is intermediary between T_g and T_x, to prevent rapid crystallization. Isothermal DSC runs at 571 °C of samples previously nucleated at 524 °C are shown in Fig. 4. The time required for each sample to crystallize completely was read immediately after the end of the crystallization peak of the corresponding isothermal DSC curve. Note, in Fig. 4, that the crystallization peak became sharper and the time required for the sample to crystallize fully diminished when the nucleation time was extended from 6 to 48 h, due to the increase in nuclei volume concentration.

A glass–ceramic was also obtained by a single heat treatment at 618 °C, for comparison with previous results reported by Fu [13]. However, based on results of heat treatments at 571 °C, the time applied to fully crystallize the sample at 618 °C was 30 min rather than the 12 h reported by the aforementioned author. Fig. 5 shows the glass–ceramic microstructures obtained after these heat treatments.

Fig. 6 shows the X-ray diffraction patterns of the glass–ceramics. In all the cases, peaks in the X-ray spectra match the Nasicon $Li_2[Ge_2(PO_4)_3]$ structure (JCPDS card 80–1924).

3.4. Electrical conductivity

Glass–ceramics with different microstructures were subjected to impedance measurements. As an example, Fig. 7 contains complex impedance plots taken at different temperatures of a glass–ceramic obtained with 6 h of nucleation (524 °C) followed by 80 min at 571 °C (microstructure in Fig. 5(a)). Sample's electrical resistance was taken at the low frequency intercept of the arc of the circle with the real axis. The electrical conductivity was then calculated and results presented in an Arrhenius plot (Fig. 8) at the Section 4.

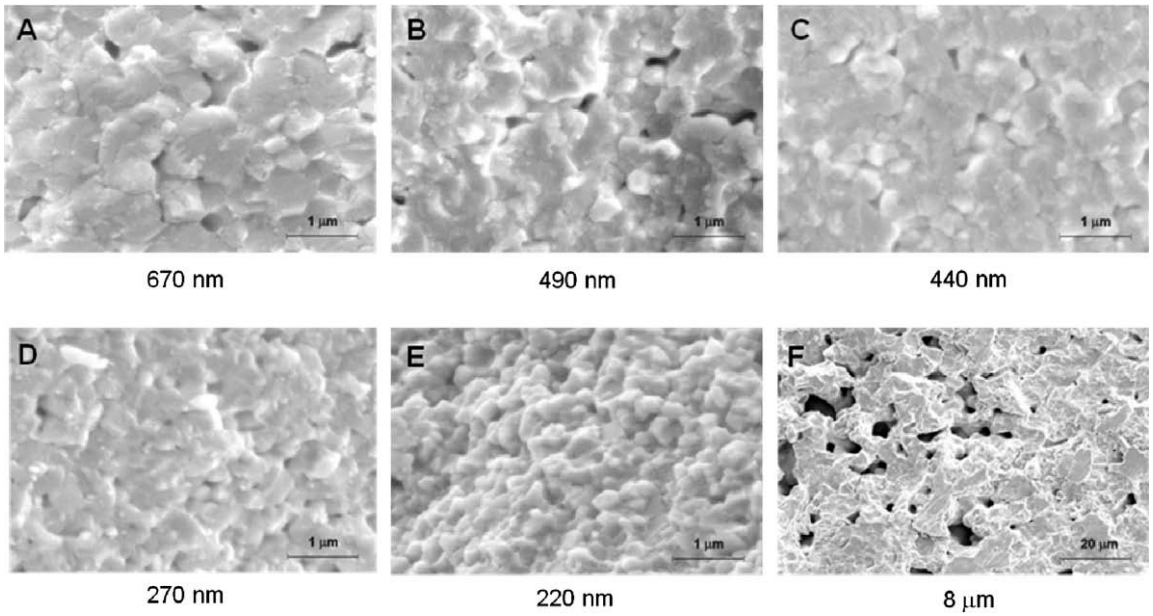

Fig. 5. Microstructure of glass–ceramic obtained by double heat treatments: (a) 6 h/524 °C + 80 min/571 °C; (b) 12 h/524 °C + 80 min/571 °C; (c) 18 h/524 °C + 60 min/571 °C; (d) 24 h/524 °C + 60 min/571 °C; (e) 48 h/524 °C + 30 min/571 °C; and (f) single heat treatment at 618 °C for 30 min. The average grain sizes are indicated.

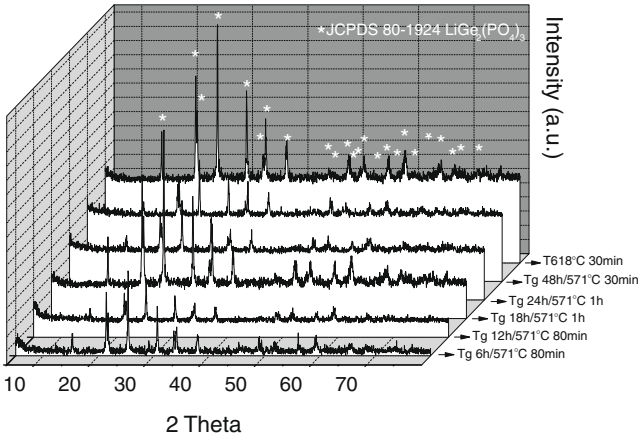

Fig. 6. X-ray diffraction patterns of $Li_{1.5}[Al_{0.5}Ge_{1.5}(PO_4)_3]$ glass–ceramics obtained by double heat treatments: glass was nucleated at T_g (524 °C) during 6, 12, 18, 24, 48 h. Crystals were subsequently grown at 571 °C during indicated periods of time. It is also shown the X-ray pattern for a glass–ceramic obtained by single heat treatment at 618 °C, during 30 min.

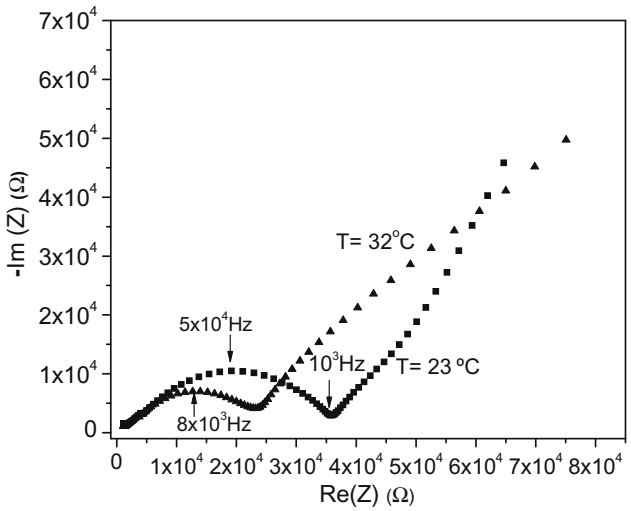

Fig. 7. Impedance plots at different temperatures of a glass–ceramic obtained by double thermal treatment for 6 h at T_g and 80 min at 571 °C.

4. Discussion

4.1. Homogeneous nucleation and temperature of maximum nucleation rate

In Fig. 1, the coincidence of the DSC crystallization peaks for monolithic and powder samples are a strong indication that this glass nucleated internally. Had surface crystallization predominated, the DSC crystallization peak of the powder sample would be sharper and shifted to lower temperatures when compared to that of the monolithic sample [20].

In Fig. 2, the DSC crystallization peak moved to lower temperatures when the nucleation temperature rose to approximately the T_g level, after which there was no significant change in the peak position with further rises in nucleation temperature (into the error limits for the differential scanning calorimeter). The intensity of the crystallization peak apparently increased and saturated in the same way. The unchanged peak intensity when the nucleation temperature rose above T_g indicates that no significant crystal growth occurred within the temperature range of the experiment. If crystal growth increased in response to higher temperatures in the nucleation step, one would expect to see a corresponding decrease in the intensity of the crystallization peak in DSC. The apparent saturation of the maximum temperature of the DSC crystallization peak at temperatures higher than 524 °C can thus be attributed to the effect of extra nucleation on the heating path before the nucleation treatment or during the subsequent non-isothermal DSC run. For treatments at temperatures above the maximum nucleation rate, such a maximum is always crossed on heating and, if the heating rate is not fast enough, significant and approximately constant nucleation can be achieved on the heating path, leading to the saturation level observed. In fact, the saturation onset temperature in Fig. 3 is a good estimation of the temperature of the maximum nucleation rate.

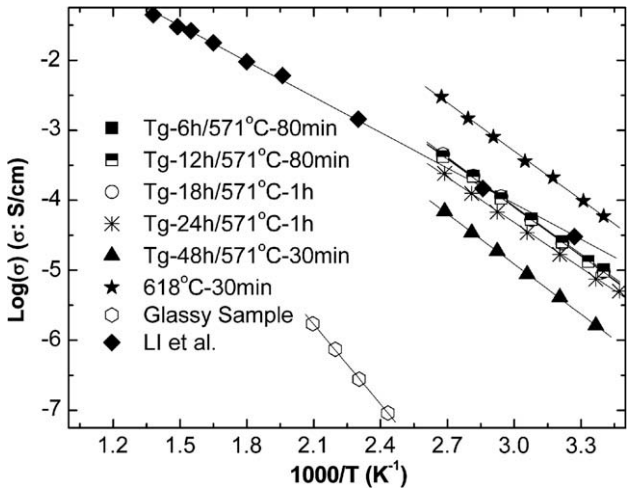

Fig. 8. Arrhenius plot of the precursor glass and glass–ceramics obtained with different heat treatments. For comparison, results from Li et al. [3] are also indicated. Lines represent the linear regression. Correlation coefficients are higher than 0.997.

The spectra in Fig. 6 indicate single phase materials, corroborating the results of dynamic DSC runs shown in Fig. 1 and the isothermal DSC results depicted in Fig. 4, which show mainly single exothermic crystallization peaks. In Fig. 1, the endothermic melting peak spread over ~40 K is typical of the melting of a non-stoichiometric or solid solution composition [25], which occurs with compositional changes as the temperature rises to the liquidus [25]. A solid solution must be present, since XRD evidences the formation of single phase materials. The aluminum–germanium substitution does not modify the position of the XRD peaks when compared to the $LiGe_2(PO_4)_3$ due to the similarity between the Al^{3+} and Ge^{4+} ionic radius. Those results are congruent with previous data obtained from sintered ceramics [3].

4.2. Glass thermal stability

The characteristic DSC temperatures of the precursor glass (Table 3) enabled us to calculate the values of glass stability parameters such as $(T_x - T_g)$ [21], Hrüby's parameter $K_H = \frac{T_x - T_g}{T_m - T_x}$ [22] and the reduced glass transition temperature $T_{gr} = T_g/T_m$ (temperatures in Kelvin). The higher the $T_x - T_g$ and the Hrüby parameter are the more stable the glass is against crystallization. The resulting parameters, which are shown in Table 3, are compared with other homogeneous nucleating glasses [21] including also, for comparison, a $Li_2[Ge_2(PO_4)_3]$ glass produced in the present work according to the melting procedures presented earlier. The data in Table 3 indicate that the glass composition under study is not a good glass forming liquid. It was experimentally observed, during the glass synthesis, that the poured liquid presented low viscosity at the process temperature, which confirms the assumption of poor glass former. The value of $T_{gr} = 0.57$ below 0.60 suggests that internal (supposedly homogeneous [23]) nucleation prevailed [23,24], as indicated by the DSC patterns of bulk and powder samples displayed in Fig. 1.

Additionally, it is interesting to note that the thermal stability parameters of the $Li_{1.5}[Al_{0.5}Ge_{1.5}(PO_4)_3]$ glass were close to those of fresnoite glass ($Ba_2TiSi_2O_8$), which presents the highest maximum nucleation rate ever determined for a glass [26]. In fact, the sharp crystallization peaks in Fig. 1 indicate a rapid crystallization process. The substitution of germanium for aluminum in the base glass increased all its stability parameters (Table 3). It is worth mentioning that, despite the low stability parameters found in the glasses investigated here, we were able to control their crystallization by double heat treatments. This fact indicates minimum overlap of the nucleation and growth rate curves as a function of temperature.

4.3. Glass–ceramic microstructure

Crystals nucleated at T_n (the nucleation temperature) are later grown at $T_{cg} > T_n$ (T_{cg} is the crystal growth temperature). If the curves of nucleation and growth rates as a function of temperature do not overlap significantly, as must be the case of the glass studied here, one can design the microstructure so that maximizing the nuclei concentration produces glass–ceramics with a minimal average crystal size, since the crystals stop growing when they impinge upon each other. On the other hand, in a microstructure with fewer nuclei, the crystals grow larger before touching their neighbors, resulting in a coarser average grain size.

Thus, as predictable, the average grain size diminished with increasing nucleation time (Fig. 5), varying from approximately 220–670 nm (estimated from the micrographs). Glass–ceramics obtained with a single heat treatment (30 min at 618 °C) presented a much larger average grain size of about 8 μm.

As expected, the glass–ceramics density was greater than that of the parent glass. In the present case, the change in density after crystallization reached more than 8% (Table 2). Such difference in density is undoubtedly a cause of pore formation. However, the glass–ceramics obtained with the double heat treatment were denser than that obtained with the single treatment. These results are clearly visible in the SEM micrographs, Figs. 5(e) and (f), which show much higher porosity in the sample obtained through the single heat treatment. Thus, although the porosity resulting from the difference in density between the glassy and crystalline phases can be predicted in glass–ceramics [27,28] the percentage and size of the pores may vary and can be controlled by the heat treatment procedure, with small grains tending toward lower porosity. The higher porosity in the sample subjected to the single heat treatment may be attributed to the reduced number of pre-existing nuclei, which leads to more residual glass entrapped among grains than in a material whose volume contained more nuclei prior to crystal growth. After the crystals impinge, the material no longer shrinks and further crystallization and densification of the residual glass among grains leads to the formation of pores in these sites to compensate for the fixed volume.

It is supposed that the crystallized volume fraction of all investigated glass–ceramics approximates 100%, i.e., if there is some glassy phase, it is merely residual. If some glassy phase is present, its percentage is below the X-ray detection, since the X-ray diffrac-

Table 3
Characteristic temperatures, $T_x - T_g$, Hrüby parameter (K_H) and T_{gr} for $Li_{1.5}[Al_{0.5}Ge_{1.5}(PO_4)_3]$, $Li[Ge_2(PO_4)_3]$ and other internal nucleating glasses.

Glass composition	T_g (K)	T_x (K)	T_m (K)	$T_x - T_g$ (K)	K_H	T_{gr}	References
$Li[Ge_2(PO_4)_3]$	849	913	1503	64	0.11	0.56	This work
$Li_{1.5}[Al_{0.5}Ge_{1.5}(PO_4)_3]$	797	877	1403	89	0.17	0.57	This work
$Ba_2TiSi_2O_8$	980	1068	1703	88	0.14	0.57	Cabral et al. [21]
$Na_2O.2CaO.3SiO_2$	854	1016	1557	162	0.30	0.55	Cabral et al. [21]
$Li_2O.2SiO_2$	733	937	1303	204	0.56	0.56	Cabral et al. [21]

togram (Fig. 6), does not show the characteristic halo of amorphous material at low diffraction angles. Furthermore, it can be noted that the duration of the employed experimental heat treatment at 571 °C far exceeds the necessary time to fully crystallize the sample, indicated by the isothermal DSC curves on Fig. 4.

4.4. Electrical conductivity

Impedance complex planes, as shown in Fig. 7, were used to calculate electrical conductivity. At higher frequencies, the impedance plot is characterized by the presence of the distorted arc of circle, indicating the presence of two phenomena with different time constants usually attributed to grain and grain boundary. The low frequency response is a straight line due to the electrode polarization characteristic of ionic conductive materials. Therefore, the total resistance (R_T) of the sample was taken as the real part of impedance (Re(Z)) corresponding to the minimum of the imaginary part (−Im(Z)) between the material and the electrode responses. Hence, the material's apparent conductivity (σ_a) is calculated by:

$$\sigma_a = \frac{1}{R_T} \cdot \frac{l}{S}, \tag{1}$$

where l is the sample's thickness and S is the electrode's surface area.

Depending on the heat treatment, impedance plots with two arc of circle were also obtained at room temperature. However, also in these cases, it was not possible to separate the grain and grain boundary contributions, since, increasing temperature the two semicircles vanished, again forming a distorted one [29]. The appearance of one or two semicircles in the impedance plots will be the subject of a further study.

The electrical conductivity of the precursor glass and the investigated glass–ceramics are depicted in an Arrhenius plot in Fig. 8, together with results from sintered ceramics obtained by Li et al. [3]. Fig. 8 illustrates a noteworthy fact, namely, that by employing the glass–ceramic route discussed here we obtained a more conductive material than that obtained by Li et al. [3] by the sintering route. However, the highest electrical conductivity reached by Fu [13] was not reproducible.

The straight lines obtained in the Arrhenius plot allow us to express the apparent conductivity as a function of temperature according to the relationship:

$$\sigma_a = \sigma_0 \exp\left(-\frac{E_a}{kT}\right), \tag{2}$$

where E_a is the activation energy of conduction, σ_0 is the so-called pre-exponential term, and k and T have their usual meanings. Table 4 lists the experimental values of σ_0 and E_a obtained from the linear regression of the experimental data. Values of activation energy are in accordance with previous results [3,13] and log σ_0 values are around 2, which is typical of most solid electrolytes [30]. The fact that log σ_0 does not change significantly when the glass crystallizes infers that microscopic parameters included in σ_0, i.e. the attempt frequency and the jump distance, do not change after crystallization. This assumption is consistent with the fact that short range order in glass and crystal are similar.

Table 4
Electrical conductivity at room temperature (σ_{25} °C), activation energy (E_a) and logarithm of the pre-exponential factor (log σ_0) of precursor glass and glass–ceramics obtained by different heat treatments.

Heat treatment	σ_{25} °C (10^{-5} S/cm)	E_a (eV)	Log σ_0 (σ_0 in S/cm)
Annealed glass	9.8×10^{-7}	0.80 ± 0.01	2.6
524 °C/6 h + 571 °C/80 min	1.9	0.420 ± 0.004	2.4
524 °C/12 h + 571 °C/80 min	2.3	0.46 ± 0.02	3.1
524 °C/18 h + 571 °C/1 h	2.0	0.42 ± 0.01	2.4
524 °C/24 h + 571 °C/1 h	1.3	0.39 ± 0.01	1.7
524 °C/48 h + 571 °C/30 min	2.0	0.390 ± 0.003	1.9
618 °C/30 min (single heat treatment)	7.6	0.46 ± 0.02	3.6

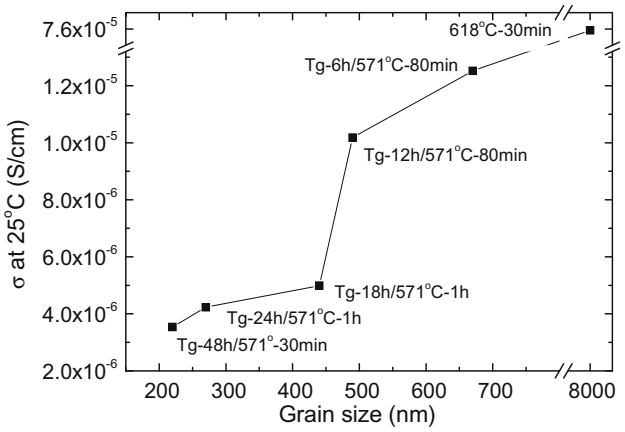

Fig. 9. Electrical conductivity at 25 °C vs. average grain size of glass–ceramics obtained by different heat treatments. Line is drawn as guide to the eyes.

The graph of the variation of electrical conductivity at room temperature *versus* average grain size in Fig. 9 was constructed based on the average grain size measured from the SEM micrographs (Fig. 5). The graph clearly indicates that the electrical conductivity increased as the grain size augmented. Conductivity values of the glass–ceramics obtained by single heat treatment approach those obtained by Xu et al. [17] and Leo et al. [15] in similar systems. The glass–ceramics obtained by these authors [17,15] exhibited average grain size of hundreds of nanometers, similar to the grain size of the glass–ceramic obtained in this work by single heat treatment (Fig. 5). Since the disordered nature of grain boundaries would destroy the conductive paths of the highly conductive Nasicon structure, a lower electrical conductivity is expected at the grain boundaries. Thus, the behavior depicted in Fig. 9 is quite expected, since the volumetric contribution of the grain boundaries increases as the grain size decreases. It is also worthy to say that, if some non-detectable residual glassy phase remains, it would have the same effect as the grain boundary. Therefore, in this system, nanometric grain sizes do not favor electrical conductivity, contrary to results reported for other ceramic materials such as ceria [31,32], which may present electronic and ionic conductivity. Indeed, Tuller [33] recently discussed the ambiguity of such results. It is interesting to note that, in the case of glass–ceramics presented here, samples with the largest grains showed the highest conductivity, despite their increased porosity. This fact leads us to conclude that the grain boundary had a more deleterious effect on the samples' conductivity than the porosity. Theoretically, the porosity would not affect electrical conductivity if the grains remain in close contact and percolate [34]. However, one must keep in mind that porosity is not suitable in a solid electrolyte applied in lithium batteries, since it can lead to the growth of lithium dendrites along the open pores at the electrode/electrolyte interface, causing short circuits and reducing the battery's service life. Thus, a good compromise between grain size and porosity must be achieved through double heat treatments.

5. Conclusions

Internal nucleation was shown to prevail in a glass with $Li_{1.5}[Al_{0.5}Ge_{1.5}(PO_4)_3]$ composition. Therefore, compositions in the $Li_{1+x}[Al_xGe_{1-x}(PO_4)_3]$ system represent a new family of internally

nucleating glasses. Although the $Li_{1.5}[Al_{0.5}Ge_{1.5}(PO_4)_3]$ glass presents low thermal stability parameters compared with other self-nucleating glasses, it was possible to control its crystallization process by double heat treatments. The resulting glass–ceramics had average grain sizes varying from 200 to 670 nm, while a single heat treatment produced a glass–ceramic with an average grain size of 8 μm. The single heat treatment led to glass–ceramic with increased porosity. However, electrical conductivity increased with increasing grain size, indicating that grain boundaries have a more deleterious effect than other microstructural factors such as porosity. Grain size thus plays an important role in the electrical conductivity of ionic conductive ceramics with Nasicon structure and can be controlled by the glass–ceramic route. Such route leads to more conductive materials than the same ceramic composition obtained by traditional powder sintering. Double heat treatments provide a compromise between grain size and porosity.

Acknowledgements

The authors are indebted to I.G. Polyakova (Institute of Silicate Chemistry, St. Petersburg, Russia) and to Professor J.L. Souquet (LEPMI, ENSEEG, Grenoble, France) for their invaluable and insightful discussions. The Brazilian research funding agencies FAPESP and CNPq are also acknowledged for their financial support.

References

[1] P. Birke, F. Salam, S. Döring, W. Weppner, Solid State Ionics 118 (1999) 149.
[2] M. Cretin, P. Fabry, J. Eur. Ceram. Soc. 19 (1999) 2931.
[3] S. Li, J. Cai, Z. Lin, Solid State Ionics 28–30 (1988) 1265.
[4] H. Aono, E. Sugimoto, Y. Sadaoka, N. Imanaka, G. Adachi, J. Electrochem. Soc. 136 (2) (1989) 590.
[5] H. Aono, E. Sugimoto, Y. Sadaoka, N. Imanaka, G. Adachi, J. Electrochem. Soc. 137 (4) (1990) 1023.
[6] H. Aono, E. Sugimoto, Y. Sadaoka, N. Imanaka, G. Adachi, Bull. Chem. Soc. Jpn. 65 (1992) 2200.
[7] H. Aono, E. Sugimoto, Y. Sadaoka, G. Adachi, J. Electrochem. Soc. 140 (1996) 127.
[8] M. Sugantha, U.V. Varadaraju, Solid State Ionics 95 (1997) 201.
[9] P. Maldonado-Manso, E.R. Losilla, M. Martinez-lara, M.A.G. Aranda, S. Bruque, F.E. Mouahid, M. Zahir, Chem. Mater. 15 (2003) 1879.
[10] O. Bohnke, S. Ronchetti, D. Mazza, Solid State Ionics 122 (1999) 127.
[11] J. Fu, J. Am. Ceram. Soc. 80 (7) (1997) 1901.
[12] J. Fu, Solid State Ionics 96 (1997) 195.
[13] J. Fu, Solid State Ionics 104 (1997) 191.
[14] J. Fu, J. Mater. Sci. 33 (1998) 1549.
[15] C.J. Leo, B.V.R. Chowdari, G.V. Subba Rao, J.L. Souquet, Mater. Res. Bull. 37 (2002) 1419.
[16] X. Xu, Z. Wen, X. Gu, X. Yang, Z. Lin, Mater. Lett. 58 (2004) 3428.
[17] X. Xu, Z. Wen, X. Wu, X. Yang, Z. Gu, J. Am. Ceram. Soc. 90 (9) (2007) 2802.
[18] C.S. Ray, D.E. Day, J. Am. Ceram. Soc. 73 (1990) 439.
[19] E.B. Ferreira, E.D. Zanotto, L.A.M. Scudeller, Glass Sci. Technol. 75 (2002) 75.
[20] M.L.F. Nascimento, L.A. Souza, E.B. Ferreira, E.D. Zanotto, J. Non-Cryst. Solids 351 (2005) 3296.
[21] A.A. Cabral, A.A.D. Cardoso, E.D. Zanotto, J. Non-Cryst. Solids 320 (2003) 1.
[22] A. Hrubý, Czch. I. Phys. B 22 (1972) 1187.
[23] E.D. Zanotto, J. Non-Cryst. Solids 89 (1987) 361.
[24] E.D. Zanotto, M.C. Weinberg, Phys. Chem. Glasses 30 (1989) 186.
[25] I.G. Polyakova, E.V. Tokareva, Glass Phys. Chem. 23 (5) (1997) 354.
[26] A.A. Cabral, V.M. Fokin, E.D. Zanotto, J. Non-Cryst. Solids 343 (2004) 85.
[27] A. Watanabe, Y. Imada, S. Kihara, J. Am. Ceram. Soc. 69 (1986) C31.
[28] A. Watanabe, M. Mitsudou, S. Kihara, Y. Abe, J. Am. Ceram. Soc. 72 (1989) 1499.
[29] A.M. Cruz, A.C.M. Rodrigues, Cerâmica 53 (2007) 180 (in Portuguese).
[30] J.L. Souquet, Ionic transport in glassy electrolytes, in: P.G. Bruce (Ed.), Solid State Electrochemistry, Cambridge Press, Cambridge, 1995, p. 95.
[31] Y.-M. Chiang, J. Electroceram. 3 (1997) 205.
[32] T. Susuki, I. Kosacki, H.U. Anderson, Solid State Ionics 151 (2002) 111.
[33] H.L. Tuller, Solid State Ionics 131 (2000) 143.
[34] R. Zallen, The Physics of Amorphous Solids, Wiley-VCH Verlag, GmbH & Co. KgaA, Weinheim, 2004. p. 137.